Mechanics of granular and polycrystalline solids

Microstructural self-organization in granular materials during failure

Nejib Hadda [a,*], François Nicot [b], Richard Wan [a], Félix Darve [c]

[a] *Department of Civil Engineering, University of Calgary, Calgary, Canada*
[b] *Geomechanics Group, ETNA, Irstea, Grenoble, France*
[c] *Laboratoire Sols Solides Structures Risques, UJF–INPG–CNRS, Grenoble, France*

ARTICLE INFO

ABSTRACT

The present paper is concerned with the analysis of microstructural instabilities in granular materials and with their relation to both macroscopic localized and diffuse failure modes. A discrete-element (DEM) computer simulation of deformations in an idealized two-dimensional frictional particle assembly subject to various biaxial loadings—notably drained compression and proportional strain paths—is proposed as a prototype model to investigate the underlying physics of material failure. Based on the transfer of the second-order work criterion to the microscopic level, we seek for contacts tagged as c^- within the granular assembly that undergo instabilities during loading history. The DEM computations yield a description of failure as a microstructural self-organization process by which c^- contacts aggregate into clusters which can either grow or breakdown as the network of contacts adjusts itself to externally applied loads during deformation history. It is proposed here that there is a close relation between the clustering of c^- contacts and the resulting failure mode based on cluster size and spatial distribution. Localized deformations are found to correlate well with sustained growth of the above clusters, while diffuse failure has more to do with smaller clusters experiencing suppressed development. A comprehensive statistical analysis on the clusters lends support to this conclusion.

© 2015 Académie des sciences. Published by Elsevier Masson SAS. All rights reserved.

1. Introduction

Granular materials undoubtedly continue to fascinate researchers, even though some key constitutive properties are today well understood. In effect, much effort has been devoted to the study of segregation mechanisms during shear flow. According to numerical studies [1–4], deformation processes in a granular assembly reveal the co-existence of two separate phases: a strong phase representing quasi-linear patterns of contacting grains—the so-called force chains—that transmit the stronger normal forces within the system, and a weaker phase encompassing the remaining grains, which provides lateral stabilization to the force chains. In fact, the constitutive richness of granular material behaviour stems from the very essence of their microstructural constitution, which can be viewed as a disordered assembly of particles interacting through a simple contact law, if long-range forces are to be excluded. It would be expected generally that such a simplified description of the underlying physics would preclude any self-organization of the system. However, rich organized microstructural patterns are observed, even if the complexity of the particle shape such as surface irregularity and concavity are ignored and replaced with spherical particles. Given that granular materials are inherently disordered, they certainly find multiple

Table 1
Physical and mechanical parameters used for the discrete element model.

Particles diameter (mm)	Density (ρ) (kg/m^3)	k_n/D^* (MPa)	k_t/k_n	Friction angle (φ) (deg)
6–18	3000	356	0.42	35

* *D* denotes the mean diameter between two particles in contact.

ways to rearrange, build and adapt their fabrics in response to an external loading [5]. Here, fabric refers to the topological construct of the contacts between particles. Thus, in the absence of disorder as in quasi-crystalline materials, most of the above salient constitutive features would disappear.

During the past several decades, there has been a great interest in the occurrence of various classes of failure in granular materials [6–11]. While soils can be regarded to some extent as a granular material, this interest was partly justified by the crucial need to better predict and describe gravity-driven phenomena such as rockfalls and landslides. In the middle of the last century, since the pioneering contribution of Hill (1958) [12], many studies have treated failure based on different approaches. In particular, the following basic questions were raised: (i) which class of failure (localized versus diffuse) should occur, (ii) can failure be properly described as a bifurcation problem, and (iii) what are the microstructural origins of failure?

Even though much effort has been expended to address these questions, they remain widely open and require further inquiry. Hence, the purpose of this paper is to probe deeper into the above-mentioned questions following a micromechanical approach. It is shown that various features of failure can be formally checked numerically using an appropriate discrete element code. Just as well confirmed by laboratory experimental tests [13], different modes of failure appear according to the loading path considered. In some cases, the computed strain field presents a chaotic pattern, with no visible sign of structuring. In other cases, localized deformations develop clearly into a shear band [14,15]. As another goal of this paper, we wish to investigate what are the microstructural ingredients that could explain why the deformation of the material localizes or not. For this purpose, material failure is described as a bifurcation process within the general framework of the second-order work theory [9,11]. According to the load-control program, the constitutive response of the material can bifurcate from a quasi-static regime towards a dynamical one [11,16]. This approach was shown to be a powerful mechanical framework that describes most of the failure modes observed before the conventional plastic limit is reached. Furthermore, taking advantage of a micromechanical approach, a microscopic formulation of the second-order work can be proposed [17] to bridge the macroscopic scale to relevant local scales. In particular, the formulation enables us to identify specific contacts associated with a negative local second-order work. These contacts are thought to play a basic role in the development of a failure mode within the material. As such, in this work, we investigate how these particular contacts emerge and evolve within the granular assembly, following a self-organization process, to eventually cluster into mesoscopic structures, the size of which determines the occurrence and the nature of failure [18].

Throughout the paper, both δ and Δ notations stand for time derivatives. They are used, according to the context, to denote infinitesimal and numerical incremental variations respectively.

2. Discrete element modelling

In this numerical study, a two-dimensional discrete element [19] model of a granular packing was considered in order to examine the link between the macro- and micro-scales in terms of instability and the ensuing mode of failure, namely diffuse or localized. The discrete element open source code 'Yade' [20] was used to perform the numerical simulations presented in this paper.

The granular packing was initially generated as a cloud of non-touching particles enclosed within four rigid frictionless walls. Then the granular assembly was subjected to a confining pressure $\sigma_2 = 300$ kPa by moving the walls towards the center at a constant rate until the isotropic state is reached. A cohesionless contact law was used to describe the interaction between the particles. It is based on three mechanical parameters: a normal contact stiffness (k_n), a tangential contact stiffness (k_t) and a friction angle (φ) introduced at the contact level through the Coulomb friction law governing the sliding between particles. The damping coefficient λ^a accounting for Cundall's non-viscous damping [21] was set to 0.05 for all simulations. The mechanical parameters of the granular packing are outlined in Table 1.

It is well recognized that the emergence of either localized or diffuse modes of failure in a granular assembly is related to the loading path followed during the test. For instance, dense sands are more likely to undergo localized failure in the form of one or more shear bands around the limit stress state during a drained compression as demonstrated through several studies [22–25]. On the other hand, diffuse failure can also be observed for the same dense sand along dilatant proportional strain or mixed (stress–strain) paths as long as the material stress response path is strictly inside the Mohr–Coulomb limit.

In the above, a dilatant proportional loading involves a constant parameter $R < 1$ constraining the lateral strain to evolve proportionally to the axial strain such that $\varepsilon_2 = -\varepsilon_1/R$. However, for a dense sand, an exceedingly low R must be chosen in order to avoid the material stress response path reaching the plastic limit condition, which would readily lead to localization. Thus, to explore the characteristics of both localized and diffuse modes within the context of the above-mentioned cases, we adopt two grain assemblies G_1 and G_2 subjected to two different loading paths in the subsequent discrete element modelling. Specimen G_1 represents a 'dense' sand ($e = 0.174$) subjected to a drained compression, while G_2 refers to a

Table 2

Physical properties of each specimen at the isotropic state.

	G_1	G_2
Height/width (h/w)	1.85	1.35
Void ratio (e)	0.174	0.217
Coordination number (z)	4.2	3.36
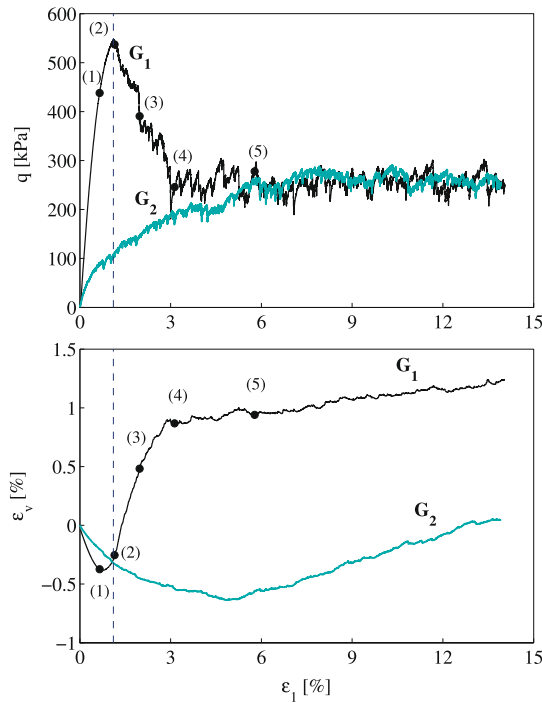
Fig. 1. (Color online.) Evolution of the deviatoric stress q and the volumetric strain ε_v in terms of the axial strain ε_1 along the drained biaxial compression for both specimens G_1 and G_2.

'medium dense' sand ($e = 0.217$) to which a dilatant proportional strain loading is applied such that $R = 0.8$. The physical characteristics of each specimen at the isotropic state are given in Table 2.

3. Localized/diffuse failure

In order to observe both modes of failure, the dense specimen G_1 was subjected to a drained biaxial compression (axially strain controlled) and the medium dense specimen G_2 was subjected to a proportional strain loading path with $R = 0.8$.

Fig. 1 shows a typical behaviour of a dilatant dense dry sand through the evolutions of both deviatoric stress $q = \sigma_1 - \sigma_2$ and volumetric strain ε_v in terms of the axial strain ε_1 resulting from the biaxial drained compression carried out on G_1. The limit stress state is marked by a distinctive peak, after which a sharp decrease in the axial stress is observed. For comparison purposes, the drained biaxial compression response of G_2 is also given in Fig. 1, where the deviatoric stress exhibits no apparent peak, but rather a plateau, while the volumetric dilatancy is retarded and only emerges after a contractancy at 5% of axial strain.

The peak in the deviatoric stress versus axial strain curve in fact refers to a limit stress state coinciding with the vanishing of the second order work W_2 [12]. According to [9], the second-order work W_2 can be expressed as

$$W_2 = \delta\sigma_1\delta\varepsilon_1 + \delta\sigma_2\delta\varepsilon_2 = \delta\varepsilon_1(\delta\sigma_1 - \delta\sigma_2) + \delta\sigma_2(\delta\varepsilon_1 + \delta\varepsilon_2)$$

$$= \delta\varepsilon_1\delta q + \delta\sigma_2\delta\varepsilon_v \tag{1}$$

Since $\delta\sigma_2 = 0$ along a drained compression, W_2 reduces to

$$W_2 = \delta\varepsilon_1\delta q \tag{2}$$

Thus,

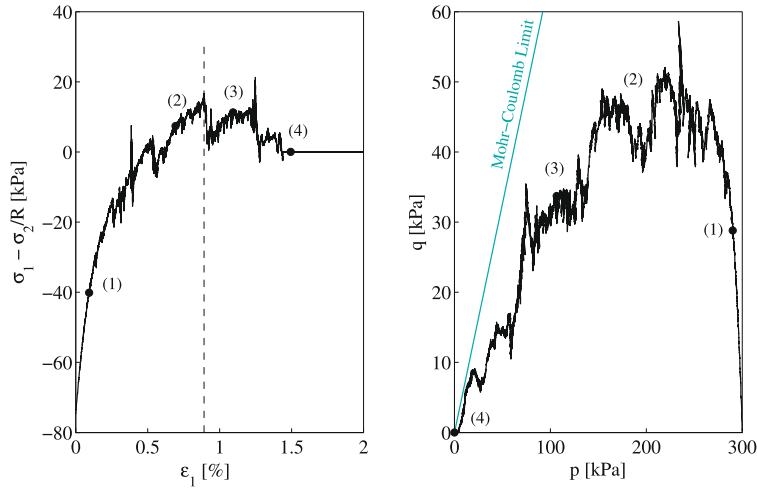$$W_2 = 0 \quad \text{implies} \quad \frac{\delta q}{\delta\varepsilon_1} = 0 \tag{3}$$

Fig. 2. (Color online.) Evolution of the stress quantity $\sigma_1 - \sigma_2/R$ and the deviatoric stress q in terms of the axial strain ε_1 and the mean pressure p respectively along the proportional strain loading path ($R = 0.8$) performed on the medium dense specimen G_2.

In contrast to the drained response of G_1, we now consider the response of G_2 along a dilatant proportional strain path where the second-order work can be written as:

$$W_2 = \delta\varepsilon_1\left(\delta\sigma_1 - \frac{\delta\sigma_2}{R}\right) + \frac{\delta\sigma_2}{R}(\delta\varepsilon_1 + R\delta\varepsilon_2) \tag{4}$$

Since $\delta\varepsilon_1 + R\delta\varepsilon_2 = 0$ along a proportional strain loading path, W_2 reduces to

$$W_2 = \delta\varepsilon_1\left(\delta\sigma_1 - \frac{\delta\sigma_2}{R}\right) \tag{5}$$

Hence,

$$W_2 = 0 \quad \text{implies} \quad \frac{\delta(\sigma_1 - \sigma_2/R)}{\delta\varepsilon_1} = 0 \tag{6}$$

Thus, a peak in the stress quantity $\sigma_1 - \sigma_2/R$ plotted against axial strain ε_1 as shown in Fig. 2a indicates that a mixed limit stress state is reached, where the second-order work W_2 vanishes. It is interesting to note that this peak does not coincide with the peak of the stress response path plotted conventionally in terms of the deviatoric stress q and the mean pressure p, as seen in Fig. 2b [26]. As the stress response path is also found to be within the Mohr–Coulomb plastic limit line, this condition is more prone to diffuse failure rather than strain localization, as will be confirmed next.

In order to check whether the specimens G_1 and G_2 underwent a localized or a diffuse failure while they were subjected to a drained biaxial compression and a dilatant proportional strain loading path, respectively, the incremental deviatoric strain ($\Delta\varepsilon_{\text{dev}}$) fields were inspected at different stress–strain states chosen along the stress path response. More precisely, $\Delta\varepsilon_{\text{dev}}$ was computed between each successive pair of stress states indicated in Figs. 1 and 2.

The incremental deviatoric strain fields displayed in Fig. 3a indicate that the dense specimen G_1 succumbed to a localized failure during the drained biaxial compression. For the stress state chosen before the peak of q is reached, $\Delta\varepsilon_{\text{dev}}$ is quite homogenous with no apparent strain localization patterns. At the peak, strain localization consisting of several emerging thin shear bands can be clearly distinguished. Moreover, it can be perceived that a unique shear band eventually prevails after peak (snapshots 3 and 4). It is worth noting also that the width of the shear band slightly widens with increasing axial strain.

In contrast to the preceding drained case on G_1, the medium dense specimen G_2 definitely displayed a diffuse failure under the proportional strain path loading, since no strain localization patterns or shear band(s) were detected as illustrated in Fig. 3b. In fact, the incremental deviatoric strain fields are quite homogeneous all along the loading, while some insignificant and non-persistent strain concentrations can be spotted occasionally.

4. Failure description at the microscopic and mesoscopic scales

4.1. Second-order work from microscopic variables

Based on the second-order work criterion [12], it has been shown [17] that a link between the macroscopic and microscopic scales in terms of instability within a granular media can be established. The second-order work W_2, which is generally expressed in terms of the tensorial variables as [9]
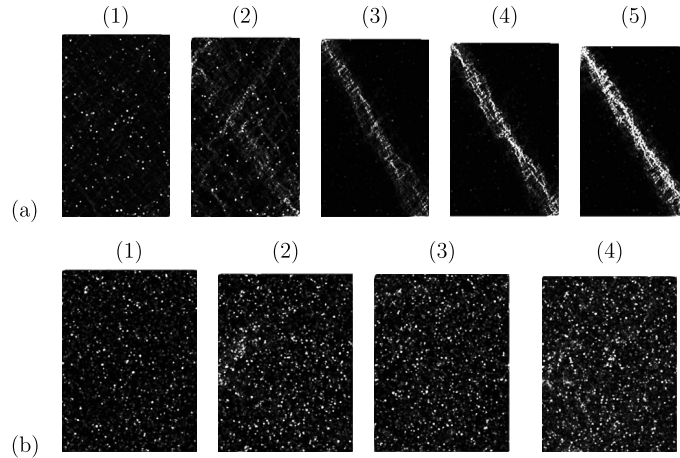
Fig. 3. Incremental deviatoric strain ($\Delta\varepsilon_{\text{dev}}$) fields computed at: (a) the stress–strain states 1 to 5 along the biaxial compression performed on the dense specimen G_1, (b) stress–strain states 1 to 4 along the proportional strain loading path performed on the medium-dense specimen G_2.

$$W_2 = \Delta\bar{\bar{\sigma}} : \Delta\bar{\bar{\varepsilon}} \tag{7}$$

where $\bar{\bar{\sigma}}$ and $\bar{\bar{\varepsilon}}$ are respectively the Cauchy stress tensor and the small strain tensor, can also be expressed in terms of the microscopic variables as [17]

$$W_2 = \sum_c \Delta\bar{f}^c \Delta\bar{l}^c + \sum_p \Delta\bar{f}^p \Delta\bar{x}^p \tag{8}$$

where $\bar{f}^c$, $\bar{l}^c$ denote the contact force and the branch vector between two particles in contact, respectively, $\bar{f}^p$ and $\bar{x}^p$ the resultant force applied on the particle p and its position vector, respectively. Since the variations implied in Eq. (7) and Eq. (8) are incremental, it is more convenient to express W_2 using an Eulerian description in this numerical study.

The second term of Eq. (8) accounts for the inertial effects to which particles may be subjected during loading. Since each loading process in this study was accomplished in the quasi-static regime, the second term of Eq. (8) can be assumed to be negligible, and therefore W_2 is reduced to

$$W_2{}^m = \sum_c \Delta\bar{f}^c \Delta\bar{l}^c \tag{9}$$

The good agreement between W_2 and $W_2{}^m$ was extensively discussed and proven numerically in [16] based on directional analyses [27] performed on dense and loose discrete element specimens. It is herein useful to generalize such finding along other loading paths, as long as quasi-static conditions prevail. In this study, a comparison between both microscopic and macroscopic second-order works is made for the drained biaxial compression performed on the dense specimen G_1; see Fig. 4. It is seen that the second-order work values, computed according to Eqs. (7) and (9) at regular intervals of axial strain are essentially identical before the limit stress state is reached, at which point W_2 vanishes and takes on negative values subsequently. After failure, a modest difference in both second-order work values may be observed, most likely due to the activation of inertial effects within the specimen, especially when it goes through sharp drops of the axial stress. Thus, it is important to include the second term of Eq. (8) while computing the second-order work from microscopic variables, when inertial effects cannot be neglected after failure has occurred.

4.2. Spatial distribution of c^- contacts during diffuse and localized failures

The microscopic form of the second-order work as given in Eq. (9) allows us to explore this quantity locally throughout a granular assembly and establish the linkage to global instability and hence failure. This local expression gives rise to the notion of second-order work at a given contact. This is meaningful as long as a granular assembly can be substituted with a system of point masses at the centroid of each connecting particle characterized by the bond (branch) vector $\Delta\bar{l}$ and associated force $\Delta\bar{f}$. As such, it is convenient to define a so-called c^- contact that denotes a contact exhibiting a negative or zero value of second-order work, i.e. $w_2 = \Delta\bar{f}^c \Delta\bar{l}^c \leq 0$. This idea was introduced in [16] where c^- contacts within a granular assembly were proven to play a major role in describing micro-instabilities in relation to the vanishing of the macroscopic second-order work.

This finding, among others, is based on a statistical study involving c^- contacts population and its spatial distribution within the specimen along all strain probe directions, especially the ones which are unstable. Directly relevant to the issue of instabilities is the investigation of c^- contacts in relation to the genesis and mode of failure in a granular assembly along different loading paths.
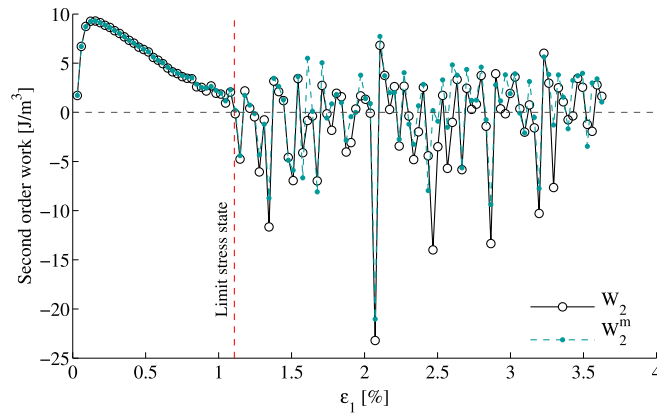
Fig. 4. (Color online.) A comparison between the second-order work computed from tensorial variables W_2 and the second-order work computed from microscopic variables $W_2{}^m$ for the biaxial compression performed on the dense specimen G_1.
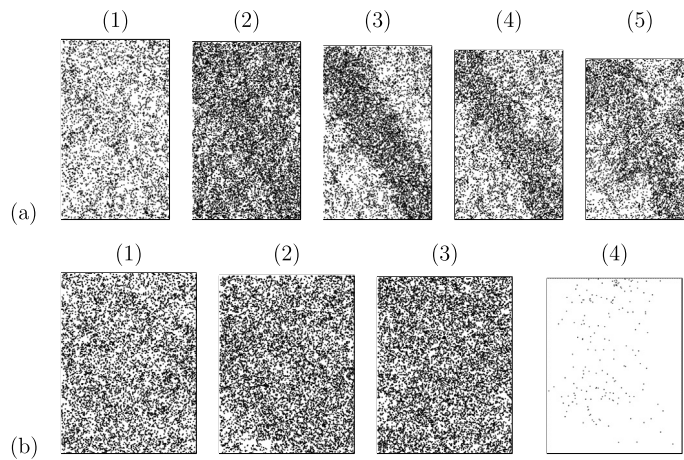

Fig. 5. Spatial distributions of c^- contacts detected at: (a) stress–strain states 1 to 5 in the biaxial compression performed on the dense specimen G_1, (b) stress–strain states 1 to 4 along the proportional stain path loading performed on the medium dense specimen G_2.

To put this into perspective, Fig. 5 shows the spatial distribution of c^- contacts, herein represented by a black dot, within both specimens at the stress states 1–5 along the biaxial compression of G_1 and stress states 1–4 along the proportional strain loading path on G_2. The correlation between the distribution of c^- contacts and the modes of failure obtained for specimens G_1 and G_2 is astounding. The strain localization pattern and the ensuing shear band observed in Fig. 3a (snapshots 2–5) through the incremental deviatoric strain ($\Delta\varepsilon_{\text{dev}}$) fields are similar to regions of concentrations of c^- contacts (Fig. 5a, snapshot (2)–(5)), except for the width of the shear band formed by c^- contacts being larger than the one revealed by $\Delta\varepsilon_{\text{dev}}$. Moreover, when the $\Delta\varepsilon_{\text{dev}}$ field is homogenous, either before the peak for localized failure (Fig. 3a, snapshot 1) or all along the proportional loading path for diffuse failure (Fig. 3b, snapshots 1–4), the distribution of c^- contacts was also found homogenous (Fig. 5b, snapshots 1–4). Notice that the snapshot 4 corresponds to a state where collapse occurred, thus the low number of c^- contacts at this state is due to the reduction of the total number of contacts.

In the light of these results, showing the possible connection of c^- contacts to the failure mode within an assembly of particles, it seems that their concentration and increase in number at failure play a major role in describing localized deformations. Nevertheless when it comes to diffuse failure, the concentration of c^- contacts seems, on the contrary, to be very limited despite their large number. Therefore, a lack of c^- contact concentration is one microscopic feature, among others, of a dilatant proportional strain path.

4.3. Aggregation of c^- contacts

The density of c^- contacts within the granular assembly and any possible aggregation can be characterized by the mean least distance $d_{\min}$ between them. As highlighted in [16], the shortening of $d_{\min}$ plays a key role in triggering instability and was proven to be very efficient in capturing variations in the total number of c^- contacts.
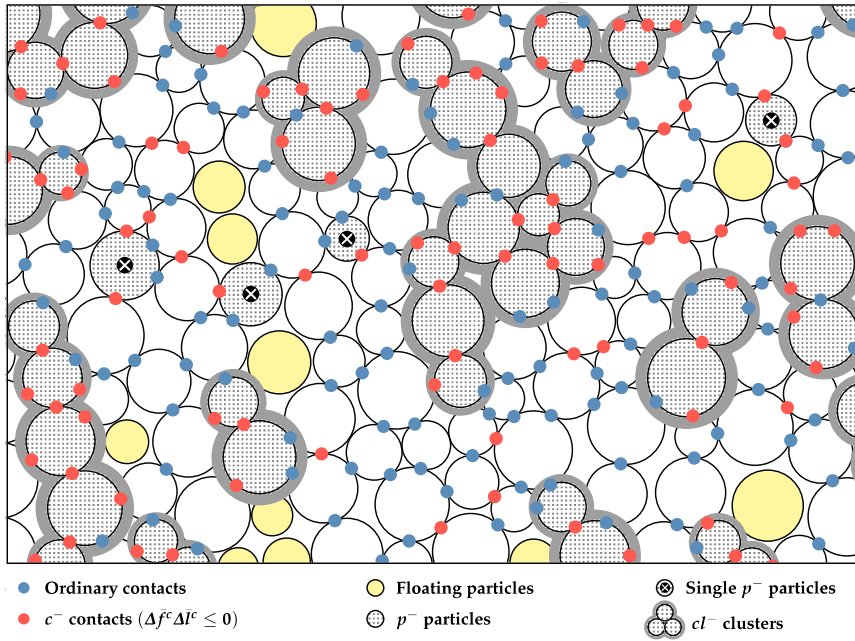
Fig. 6. (Color online.) Development of cl^- clusters based on c^- contacts and p^- particles.

As the number of c^- contacts increases within the specimen, some of them aggregate with other so as to belong to the same particle. In the extreme case, all contacts in the vicinity of a given particle p would be all of the c^- type, which necessarily implies that

$$\sum_{c \in p} \Delta \bar{f}^c \Delta \bar{l}^c \leq 0 \tag{10}$$

It is very restrictive to only consider such densest aggregation of c^- contacts in this study. Also, Eq. (10) holds true even if not all contacts are of the c^- type. Thus, it is rather more relevant to define an aggregation of c^- contacts based on the most loaded (but not necessarily fully loaded) particles (with c^- contacts). As such, a given particle p that satisfies the condition (10) is herein denoted by p^-.

Furthermore, if the particle comes into contact with at least another p^-, then it is considered as part of a cluster of particles standing for a c^- contact aggregate. Such cluster of p^- particles is denoted by cl^-.

Fig. 6 gives an illustration of cl^- clusters accounting for c^- contact aggregation within a granular assembly with respect to c^- contacts and p^- particles.

4.4. Failure description in terms of cl⁻ clusters

Every cl^- cluster is distinct and develops progressively starting from a given particle p^- as more adjoining p^- particles are found in the vicinity and added. As such, the development of cl^- clusters was studied at each stress–strain state chosen at regular intervals of axial strain along the stress response paths of the two tests (Figs. 1 and 2) studied in the paper.

4.4.1. Spatial distribution of cl⁻ clusters

Fig. 7 shows the spatial distribution of cl^- clusters for the above two tests at strategic states during loading history. It is observed that clusters mainly concentrate inside localized zones of deformation during the drained compression test in contrast to a dispersion of smaller clusters in the case of the proportional strain loading path test. Also, the examination of cl^- cluster distribution proves to be more suitable than c^- contacts (Fig. 5) to directly predict the failure mode. For instance, for localized failure, large clusters are found to be distributed within shear bands. Also, the width of the shear band characterized by cl^- clusters is more accurate and less wide than the one revealed by c^- contacts distribution (Fig. 5a), and similar to the one observed in the incremental strain fields (Fig. 3a). Moreover, the cl^- cluster spatial distribution seems to reveal the slight strain localizations occurring during diffuse failure (Fig. 3b), which are hardly distinguishable through c^- contacts distribution.
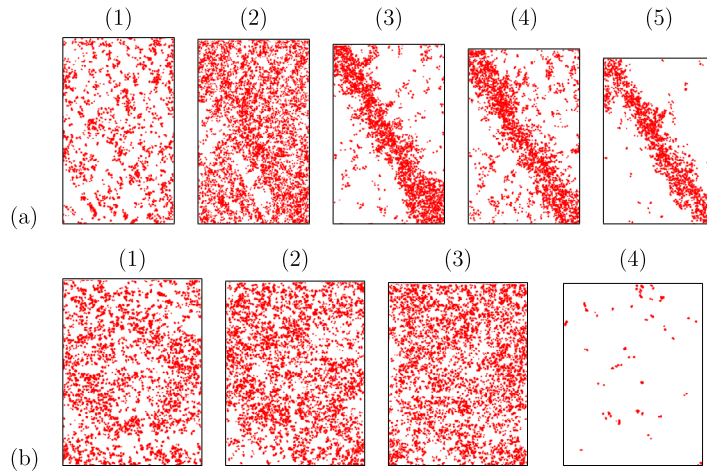
Fig. 7. (Color online.) Spatial distribution of cl^- clusters at: (a) stress states 1 to 5 along the drained compression, (b) Stress states 1 to 4 along the proportional strain loading path.
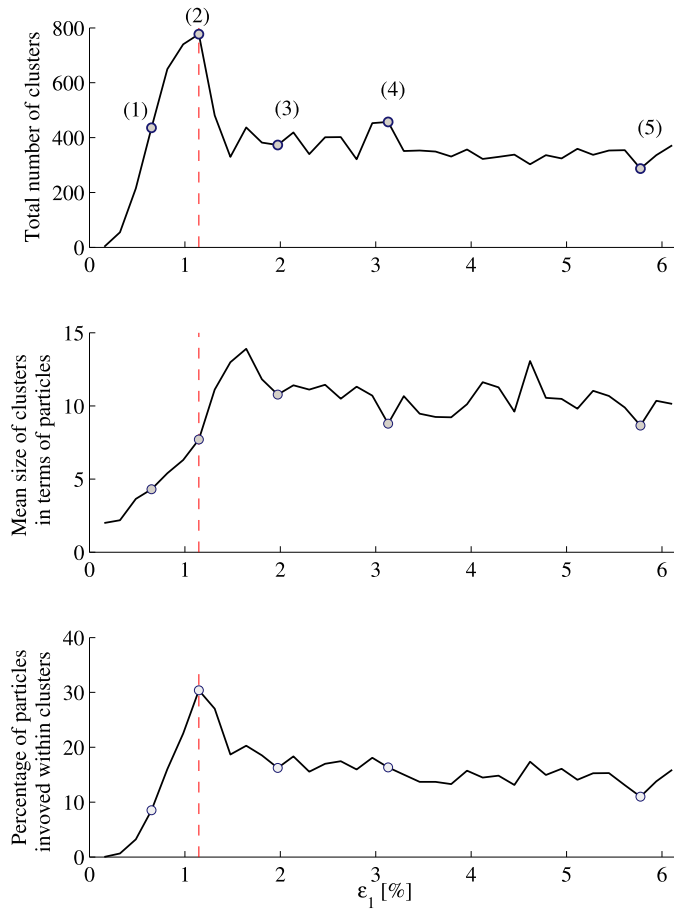

Fig. 8. (Color online.) Evolution of the number, mean size of cl^- clusters and the number of particles in all clusters in drained compression.

4.4.2. Evolution of cl^- clusters during loading history

Figs. 8 and 9 show the evolutions of the total number of cl^- clusters, their mean size in terms of number of particles, and the overall number of particles in all cl^- clusters respectively during both a localized and a diffuse failure.

In the case of a localized failure, the total number of cl^- clusters increases to reach a peak at the limit stress state (peak of the deviatoric stress q), followed by a sharp drop after which fluctuations around a constant value are observed at the
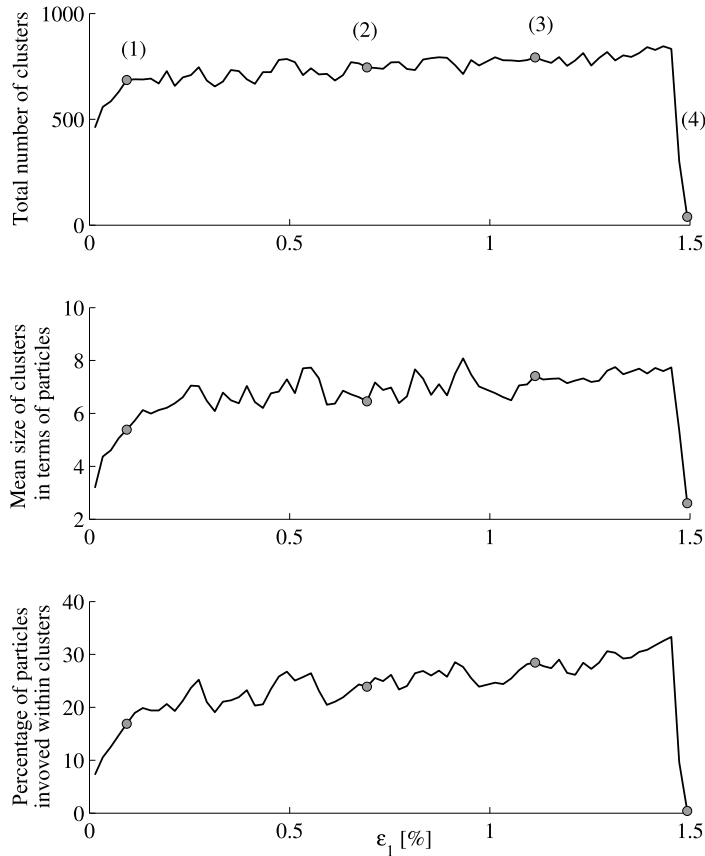
Fig. 9. Evolution of the number, mean size of cl^- clusters and the number of particles in clusters along the proportional strain loading path.

approach and during the critical state. The same trend is generally observed for the mean size of cl^- clusters and the total number of cl^- cluster particles. It is worth noting that after the limit stress state is reached, the cl^- clusters continue to grow in size while they undergo a sharp decrease in number. Under these circumstances, localized deformations evolve such that more p^- particles aggregate to form the shear band(s); e.g. see states (2) and (3) in Fig. 7a.

As shown in Fig. 9 referring to diffuse failure, there are no discernible signs of failure occurrences in the evolutions of the total number of cl^- clusters, their size and the number of particles in all clusters. The granular assembly maintains a virtually constant number of cl^- clusters throughout loading history, except towards the end when there is an abrupt drop signaling collapse. As for the mean cluster size and the number of cluster particles, there is a remarkable increase at the beginning of loading, which is thereafter subdued. In fact, the mean size of cl^- clusters fluctuates within a narrow spread whereby they seem to be restricted to grow despite modest increases corresponding to various peaks $\sigma_1 - \sigma_2/R$ back in Fig. 2. The clusters grow a bit, but not for long as they soon break down and revert to their original size. The above observations are in sharp contrast with the case of localized failure shown in Fig. 8, where growth of clusters persist. Thus, it is tempting to associate diffuse failure with the perpetual fluctuation within cl^- clusters so that they do not grow as the c^- contact population spreads throughout the network.

4.4.3. Incremental changes in cl^- cluster states

In the pursuit of further insights in the results discussed in the above, it is interesting to examine how cl^- clusters, at a given state, have evolved with respect to a previous state. Hence, five cl^- cluster state subsets are identified within the granular assembly so that their evolution from one state to another one can be followed during a given time increment Δt. Fig. 10 illustrates the above-mentioned subsets describing the possible states whereby a cl^- cluster may (1) remain constant, (2) shrink in size, (3) expand, (4) newly form, or (5) vanish. Figs. 11 and 12 show the evolutions of the number of clusters and their mean size in terms of number of particles according to the above-defined cluster state subsets for drained compression and proportional strain loading path respectively.

The disappearance of clusters and formation of new ones are found not only to be the most numerous, but also to show a constant small size (2 to 4 particles), all along with unchanged clusters, throughout the loading; see Fig. 11a and b. It is worth noting that in both figures, when the mean size of cl^- clusters for a given subset is zero, this means that the subset is void, since the mean size cannot be smaller than two by virtue of the definition of a cl^- cluster.
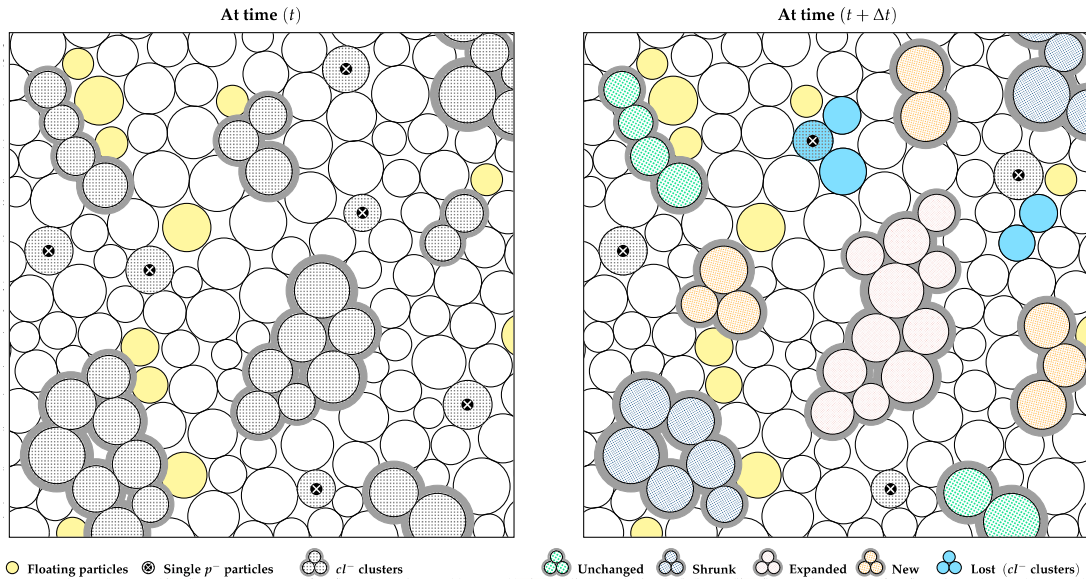
Fig. 10. (Color online.) An illustration of eligible *cl⁻* clusters subsets arising when two different states are involved for comparison.
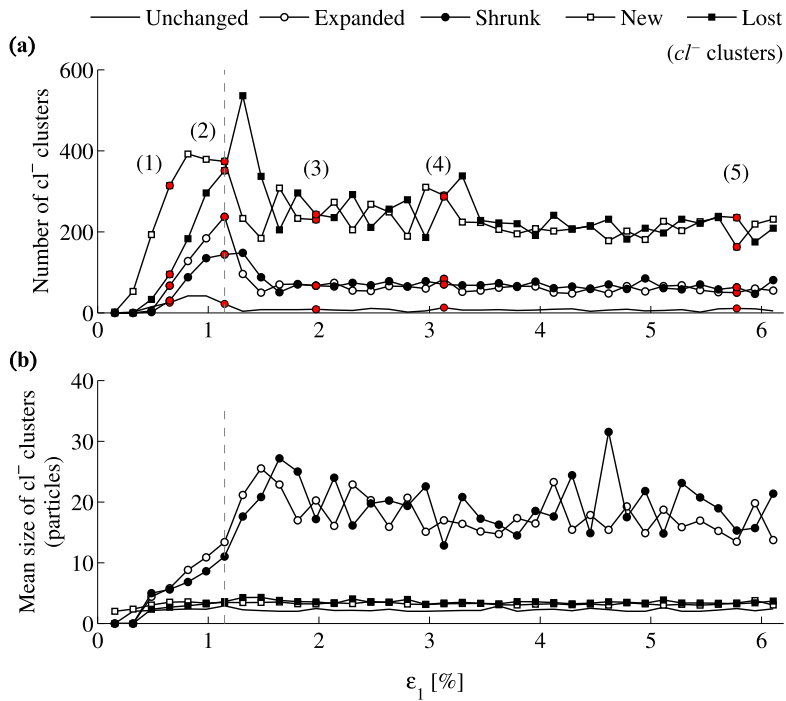

Fig. 11. (Color online.) Evolution of the: (a) number, (b) mean size of *cl⁻* clusters according to the subset to which they belong along the drained compression.

At the very beginning of the biaxial compression, the initially formed *cl⁻* clusters are small in size and can hardly survive, since the majority of them vanish. In other words, the granular assembly can easily overcome small local instabilities characterized by these tiny *cl⁻* clusters. But as the axial strain increases, the granular assembly can no longer overcome larger local instabilities characterized by both enlarged and reduced *cl⁻* clusters because instead of vanishing, they keep growing in size. Meanwhile, it still can overcome small local instabilities characterized by small clusters, since most of the lost *cl⁻* clusters are newly formed. This can be deduced from the evolution of the mean size of the enlarged and reduced *cl⁻* clusters on the one hand, and the evolution of the mean size of the equal, new and lost *cl⁻* clusters, on the other hand. Therefore, along a biaxial compression, a granular assembly can overcome local instabilities as long as they do not reach the
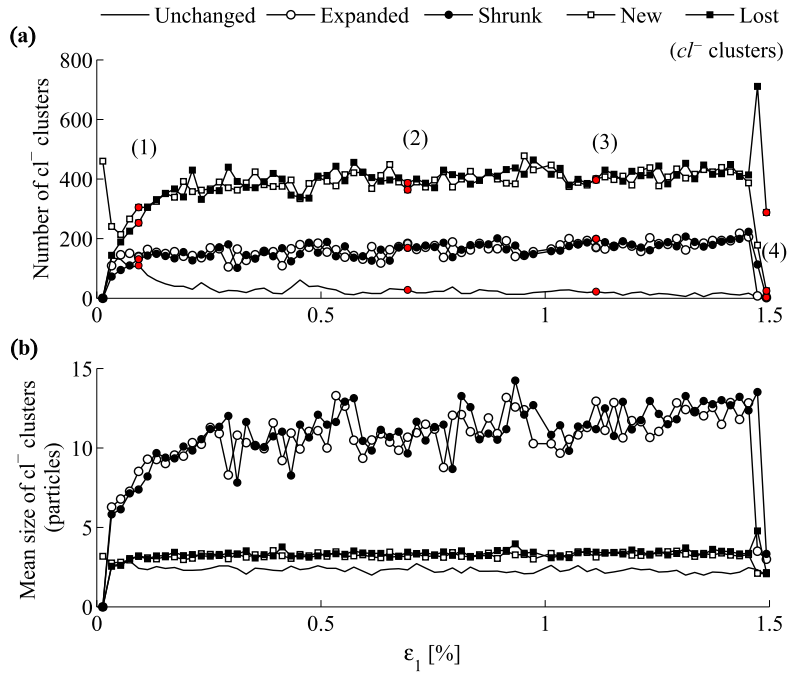
Fig. 12. (Color online.) Evolution of the: (a) number, (b) mean size of cl^- clusters according to the subset to which they belong along the proportional strain loading path.

mesoscale. The mesoscale refers here to an aggregate of particles whose size exceeds the mean size of the new or lost cl^- clusters.

The ongoing increase before the peak of the mean size of the enlarged and the reduced cl^- clusters emphasizes the fact that at an early loading stage, once a cl^- cluster reaches the mesoscale, it does not vanish, but keeps expanding in the same spatial zone, involving larger concentrations of c^- contacts. Since concentrations of c^- contacts were shown to be in line with strain localization (Fig. 5a), the emergence of such cl^- clusters can be viewed as a precursor to localized failure. Moreover, the mean size of the enlarged and the reduced cl^- clusters keep increasing after the peak, while their number decreases. As mentioned in the previous subsection, this phase corresponds to the shear band growth involving obviously only these two subsets of cl^- clusters, during which they both reach their highest mean size values, see Fig. 7a. Once the shear band is fully developed, a slight decrease in the mean size value is observed, after which this latter fluctuates around a constant value.

It is worth noting that after peak, more cl^- clusters are being lost, while the number of cl^- clusters of the all other subsets is decreasing. However, this loss only still pertains to small clusters, as shown in Fig. 11b. Thus, failure of the specimen is consistently controlled by mesoscale instabilities throughout loading history.

According to Fig. 11a and in line with Fig. 7a, the largest number of newly created clusters is observed between the states (1) and (2) before the full emergence of the shear band. Obviously, cl^- clusters can develop monotonically only within the shear band, since a large extinction of these latter is observed outside the band, notably between the states (2) and (3) where the maximum number of lost clusters is reached. This finding could qualify failure within the shear band as being of a diffuse character, as the elastic unloading experienced by particles located outside the shear band concentrates the instabilities inside the band.

In contrast to what was observed during the biaxial compression, cl^- clusters emerge abruptly from the very beginning within the specimen, while being subjected to the proportional strain loading path (Fig. 12). They soon start to occupy the constant, enlarged and reduced cl^- clusters subsets progressively while the number of the new cl^- clusters is decreasing. Thereafter, both the mean size and the number of cl^- clusters within each subset stabilize and vanish when collapse occurs, except for the mean size of the enlarged and reduced subsets, which shows a slight slow increase.

Indeed, even along a proportional strain loading path, a granular assembly can hardly recover from local instabilities when the mesoscale is reached. It should be noted in Fig. 12a and b that the number of lost and new cl^- cluster subsets coincide approximately. The same observation applies to the cl^- clusters that increase and decrease in size. Since the corresponding mean cl^- cluster size for both subsets also remain fairly constant and distinct from each other, it can be concluded that newly formed cl^- clusters at a given state are subsequently lost in the next one.

Noticeably, large cl^- clusters are quite present within the specimen, but surprisingly, they preserve the same number and the same mean size all along the loading with a limit value of approximately 10 particles. While small cl^- clusters are

more numerous, they tend to vanish instantly. Therefore, the proportional strain path seems to prevent large cl^- clusters from growing larger in number and size and limit the lifetime of small cl^- clusters.

5. Conclusions

The correspondence between the statistical distribution of unstable particle clusters and the emerging failure mode as predicted for a two-dimensional granular assembly suggests that second-order work is a basic key indicator of failure in granular materials. As new results, it is shown that:

(1) the choice of cl^- clusters as an aggregate of c^- contacts provides a powerful means to evaluate instability at the mesoscale, and hence describes the proper mode of failure observed at the macroscopic level;
(2) unlike microscopic instabilities, any instability found at the mesoscale cannot be recovered during the deformation process due to sustained growth of clusters; and
(3) the loading path controls the evolution of cl^- clusters with respect to their numbers and sizes in that clusters either grow in size, leading to strain localization in drained compression, or reach a limiting size (herein ≈ 10 particles), whereby newly formed clusters immediately breakdown in the case of proportional strain loading.

The above findings imply that granular materials respond to external loading through propagation of micro- to mesoscale instabilities attributed to the violation of second-order work at contacts. This study proves that DEM simulations, in which unstable particle clusters grow and die to the emergence of the most compatible mode of failure, essentially provide a useful method for exploring the validity of this idea. It has been shown that internal mechanics of particles based on local second-order work yield to self-organization phenomena such as aggregation of unstable particles with subsequent clustering. The statistical analysis of clustering determines whether the failure mode will be localized or diffuse in the end.

References

[1] F. Radjai, S. Roux, J.-J. Moreau, Contact forces in a granular packing, Chaos 9 (3) (1999) 544–550.
[2] A. Tordesillas, M. Muthuswamy, On the modeling of confined buckling of force chains, J. Mech. Phys. Solids 57 (2009) 706–727.
[3] A. Tordesillas, D.M. Walker, Q. Lin, Force cycles and force chains, Phys. Rev. E 81 (2010) 011302.
[4] A. Tordesillas, Q. Lin, J. Zhang, R.P. Behringer, J. Shi, Structural stability and jamming of self-organized cluster conformations in dense granular materials, J. Mech. Phys. Solids 59 (2011) 265–296.
[5] N.P. Kruyt, Micromechanical study of fabric evolution in quasi-static deformation of granular materials, Mech. Mater. 44 (2012) 120–129.
[6] D. Bigoni, T. Hueckel, Uniqueness and localization, I. Associative and non-associative elastoplasticity, Int. J. Solids Struct. 28 (2) (1991) 197–213.
[7] R. Nova, Controllability of the incremental response of soil specimens subjected to arbitrary loading programs, J. Mech. Behav. Mater. 5 (2) (1994) 193–201.
[8] F. Darve, G. Servant, F. Laouafa, H.D.V. Khoa, Failure in geomaterials, continuous and discrete analyses, Comput. Methods Appl. Mech. Eng. 193 (2004) 3057–3085.
[9] F. Nicot, F. Darve, A micro-mechanical investigation of bifurcation in granular materials, Int. J. Solids Struct. 44 (2007) 6630–6652.
[10] F. Nicot, F. Darve, Diffuse and localized failure modes: two competing mechanisms, Int. J. Numer. Anal. Methods Geomech. 35 (5) (2011) 586–601.
[11] F. Nicot, L. Sibille, F. Darve, Failure in rate-independent granular materials as a bifurcation toward a dynamic regime, Int. J. Plast. 29 (2012) 136–154.
[12] R. Hill, A general theory of uniqueness and stability in elastic-plastic solids, J. Mech. Phys. Solids 6 (1958) 236–249.
[13] A. Daouadji, F. Darve, H. Al Gali, P.Y. Hicher, F. Laouafa, S. Lignon, F. Nicot, R. Nova, M. Pinheiro, F. Prunier, L. Sibille, R. Wan, Diffuse failure in geomaterials, experiments, theory and modelling, Int. J. Numer. Anal. Methods Geomech. 35 (16) (2011) 1731–1773.
[14] J.R. Rice, The localisation of plastic deformation, in: W.T. Koiter (Ed.), Theoretical and Applied Mechanics, IUTAM Congress, 1976, pp. 207–220.
[15] R. Wan, M. Pinheiro, A. Daouadji, M. Jrad, F. Darve, Diffuse instabilities with transition to localization in loose granular materials, Int. J. Numer. Anal. Methods Geomech. 37 (10) (2013) 1292–1311.
[16] H. Hadda, F. Nicot, F. Bourrier, L. Sibille, F. Radjai, F. Darve, Micromechanical analysis of second order work in granular media, Granul. Matter 15 (2013) 221–235.
[17] F. Nicot, N. Hadda, F. Bourrier, L. Sibille, R. Wan, F. Darve, Inertia effects as a possible missing link between micro and macro second-order work in granular media, Int. J. Solids Struct. 49 (10) (2012) 1252–1258.
[18] A. Tordesillas, S. Pucilowski, L. Sibille, F. Nicot, F. Darve, Multiscale characterization of diffuse granular failure, Philos. Mag. 92 (36) (2012) 4547–4587.
[19] P.A. Cundall, O.D.L. Strack, A discrete numerical model for granular assemblies, Geotechnique 29 (1) (1979) 47–65.
[20] V. Šmilauer, E. Catalano, B. Chareyre, S. Dorofeenko, J. Duriez, A. Gladky, J. Kozicki, C. Modenese, L. Scholtès, L. Sibille, J. Stránský, K. Thoeni, Yade Documentation, The Yade Project, 2010.
[21] P.A. Cundall, A computer model for simulating progressive large scale movements in blocky rocky systems, in: Proceedings of the Symposium of the International, Society of Rock Mechanics, Nancy, France, 1971, pp. 129–136.
[22] J. Desrues, J. Lanier, P. Stutz, Localization of the deformation in tests on sand sample, Eng. Fract. Mech. 21 (4) (1985) 909–921.
[23] J. Desrues, Shear band initiation in granular materials: experimentation and theory, in: F. Darve (Ed.), Geomaterials Constitutive Equations and Modelling, Taylor and Francis Books, Elsevier, 1990, pp. 283–310.
[24] I. Vardoulakis, Shear band inclination and shear modulus of sand in biaxial tests, Int. J. Numer. Anal. Methods Geomech. 4 (2) (1980) 103–119.
[25] P.V. Lade, Localization effects in triaxial tests on sand, in: IUTAM Conference on Deformation and Failure in Granular Media, Delft, The Netherlands, 1982.
[26] F. Nicot, A. Daouadji, N. Hadda, M. Jrad, F. Darve, Granular media failure along triaxial proportional strain paths, Eur. J. Environ. Civ. Eng. 17 (9) (2013) 777–790.
[27] G. Gudehus, A comparison of some constitutive laws under radially symmetric loading and unloading, in: I.W. Wittke (Ed.), 3rd International Conference on Numerical Methods in Geomechanics, A.A. Balkema, Aachen, Germany, 1979, pp. 1309–1323.